








# Multi-Stacked High-Speed PIN-PD for Compact Mobile Optical-Wireless Transceiver

Toshimasa Umezawa , Member, IEEE, Shinya Nakajima , Abdelmoula Bekkali , Senior Member, IEEE, Michikazu Hattori, Atsushi Matsumoto , Member, IEEE, Atsushi Kanno , Senior Member, IEEE, Kouichi Akahane , and Naokatsu Yamamoto 

(Top-Scored Paper)

**Abstract**—We proposed a 0.3-mm large-aperture multi-stacked PIN-PD operated up to 20 Gbps to mitigate optical alignment tolerance in mobile optical wireless communications (OWCs). By reducing PIN junction capacitance using multi-stacked layers via fabrication, we achieved a 38-fold increase in 3 dB bandwidth (7.6 GHz) compared to a conventional 0.3-mm large PIN-PD. Assuming 10–20 km/h mobile communication applications at a short distance of 20 m, we developed a mobile OWC transceiver combined with a multi-stacked PIN-PD. In the mobile OWC demonstration considering a tracking latency of  $<5$  ms against a moving beam (1.4 km/h) at 2.1 m, we successfully achieved bit error rate levels of  $10^{-6}$  at 10 Gbps and  $<3.8 \times 10^{-3}$  at 20 Gbps on a 2.1 m long optical bench (relative speed = 13.7 km/h at 20 m) for 1 hour.

**Index Terms**—Free space, mobile, multi-stacked, optical wireless communication, PIN-PD, transceiver.

## I. INTRODUCTION

IN THE future, wireless communication networks beyond 5G (B5G), ultrahigh-speed, low-latency, cost-effective, and energy-saving communication systems will be indispensable to realize Society 5.0 [1]. Regardless of outdoor or indoor environments, advanced high-quality wireless communication services will be provided to users worldwide. To date, used frequency bands have shifted from microwave frequencies to millimeter-wave frequencies to increase the data rates of wireless communications. This trend of higher frequency band usage

Manuscript received 6 November 2023; revised 9 February 2024 and 8 March 2024; accepted 14 March 2024. Date of publication 19 March 2024; date of current version 14 June 2024. This work was conducted under the “R&D of high-speed THz communication based on radio and optical direct conversion” under contract JPJ000254 made with the Ministry of Internal Affairs and Communications of Japan. This work was supported in part by JST SICORP under Grant JPMJSC22E1, Japan. (Corresponding author: Toshimasa Umezawa.)

Toshimasa Umezawa, Shinya Nakajima, Atsushi Matsumoto, Kouichi Akahane, and Naokatsu Yamamoto are with Optical Access Technology Laboratory, The National Institute of Information and Communications Technology, Koganei-shi 184-8795, Japan (e-mail: toshi\_umezawa@nict.go.jp; n-shinya@nict.go.jp; a-matsumoto@nict.go.jp; akahane@nict.go.jp; naokatsu@nict.go.jp).

Abdelmoula Bekkali and Michikazu Hattori are with R&D Center, Toyo Electric Corporation, Kasugai-shi 486-8585, Japan (e-mail: bekkali\_a@toyo-elec.co.jp; mitikazu\_hattori@toyo-elec.co.jp).

Atsushi Kanno is with the Nagoya Institute of Technology, Nagoya-shi 466-8555, Japan (e-mail: kanno.atsushi@nitech.ac.jp).

Color versions of one or more figures in this article are available at <https://doi.org/10.1109/JLT.2024.3378721>.

Digital Object Identifier 10.1109/JLT.2024.3378721

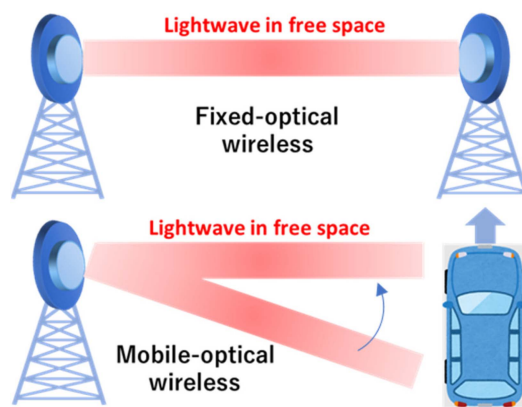


Fig. 1. Schematic illustration of fixed OWC (upper graph) and mobile OWC (lower graph).

will continue in the future as well. Frequencies below 4 GHz in LTE-advanced (4G) technology [2] have been increased to 6 GHz (SUB-6) and 28–40 GHz for millimeter waves (as a new radio band) in 5G technology [3]. According to B5G (6G) technology explained in the white paper [4], the use of extremely high-frequency D-band (110–170 GHz) [5] to achieve data rates of  $>100$  Gbps has been discussed. In addition, several studies on THz frequency communications near 300–600 GHz [6], [7] have been reported recently; these studies will be expected for usage of unused wide frequency bandwidths in the range of 300–600 GHz.

Meanwhile, optical wireless communication (OWC) technology for B5G has been studied; compared to conventional radio wireless communications, it is considered to be a more attractive alternative to improve data rates and latency [8], [9]. Moreover, OWCs can avoid interference issues [10] in radio wireless communications and secure communications [11] owing to their nondivergent laser beam characteristics. They have been demonstrated for long-range communications (more than 500 km) between the ground and satellites [12] or are planned to be extended to high-altitude platform stations [13] (HAPSs; distance = 20 km). OWCs can be applied to short- to medium-range fixed links between buildings for mobile backhaul and front-haul [14], as well as outdoor mobile links [15] (Fig. 1).

Furthermore, indoor OWCs have been considered for high-speed office [16], and factory networks for operating smart robots [17]. Moreover, under-water mobile OWC systems based on visible lightwaves have been reported considering low optical power attenuation in water [18]. Downsizing large OWC transceiver systems to compact and lightweight systems like WiFi routers would have a major impact on B5G. Here, one of bottleneck technologies to downsize OWC systems might be an optical coupling issue between transceivers. A combination of divergent beam transmission based on the LED sources of a transmitter and a large-aperture avalanche photodetector (APD) of a receiver may address the aforementioned issue; however, data rates would be limited by the narrow bandwidth of LEDs or APDs. Instead, a laser light source with a high-speed PIN-PD should be employed in high-speed OWC systems. However, the mechanical beam positioning and tracking functions in the transceivers can affect compactness and low-cost design. In particular, the volume of mechanical parts in a mobile transceiver is likely to be larger compared to a fixed OWC transceiver, thereby leading to a larger footprint. Enlarging the PD aperture size can be an effective approach to realize a compact mobile OWC transceiver.

Recently, a high-speed beam-tracking OWC transceiver with a response time of  $<5$  ms and a movable lens system was developed for demonstrating 200-m fiber-to-fiber fixed OWC [19]. This technology was applied to a mobile OWC transceiver, which was demonstrated to operate at low moving speed under the condition of relatively low optical coupling efficiency to fiber on a receiver [20]. Meanwhile, with regard to large-aperture high-speed PDs, we developed large high-speed PD array devices (0.16–0.25 mm;  $4 \times 4$  or  $6 \times 6$  array) that operated at 10–30 GHz [21] to improve the data rate and optical coupling efficiency in free space. In the demonstration of space diversity signal processing [22] and WDM signal direct detection [23], we confirmed (as a proof of concept) that the PD array device was effective and useful in improving the data rate and mitigating optical alignment tolerance in free space. In addition to the multi-parallel output-type PD array devices mentioned above, a single output-type PD array device ( $8 \times 8$ ;  $20 \times 20$ ) was developed to simplify the complexity of multioutput signal processing after O–E conversion. The large-aperture PD array device (0.4–0.8 mm), which comprised 30–40- $\mu\text{m}$  PD pixels connected in series and parallel, achieved a high 3 dB bandwidth over 10 GHz [24]. With the single output-type large PD array, a high data rate of 20 Gbps was achieved via OWC without considering beam positioning and tracking function in a 20-m free space [25]. One issue of the single output-type PD array device in above was the requirement of high fabrication yield in the  $N \times N$  PD array structure, where all  $N \times N$  small PD pixels should function properly without any defects.

In this report, we proposed a multi-stacked large-aperture PIN-PD (single output type) operated up to 20 Gbps, and a compact mobile OWC transceiver with the proposed PD device was developed. While demonstrating mobile OWC, the optical alignment robustness of the developed transceiver considering the bit error rate (BER) was discussed, assuming a moving speed

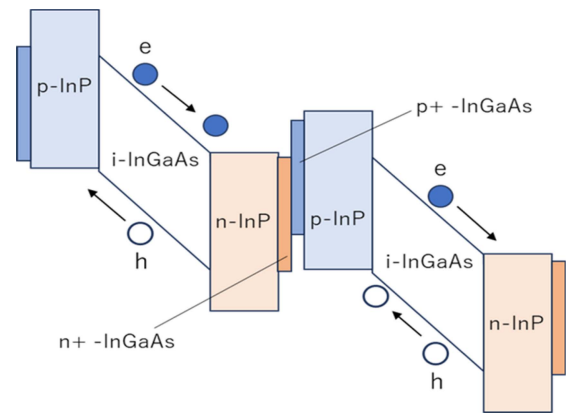


Fig. 2. Schematic energy-band diagram for the multi-stacked PIN-PD using III-V compound material (InP/InGaAs).

of 10–20 km/h at a distance of 20 m. This paper is an extension version of the top-scoring paper from ECOC 2023 [26].

## II. MULTI-STACKED PIN-PD

### A. Device Design

In a mobile OWC system, the position of the laser beam on the PD surface continuously varies, even if the beam-tracking function is installed in the laser beam based free space optical (FSO) transceiver. To address this problem, the PD aperture size needs to be increased. Considering the tradeoff relationship between the PD size and frequency response (3 dB bandwidth), it would be difficult to simultaneously satisfy the conditions of a high 3 dB bandwidth and a large aperture size. Although the 3 dB bandwidth in a PD is defined by the CR time constant and carrier traveling time, the entire bandwidth is dominated by the CR time constant, when assuming a mm to sub-mm range large aperture PD design. Therefore, reducing junction capacitance is one of the effective approaches for increasing the frequency response for large PDs.

Note; regarding the trade-off in small PDs in  $\mu\text{m}$  range, it seems possible to approximately double the photodetective area (aperture size) without affecting the 3 dB bandwidth [27].

III-V compound-based multijunction devices have been studied for VCSEL and solar-cell device applications, which enable high-power operation [28], [29] and high quantum efficiency [30], [31], respectively. High-light-emission performance through tunneling junctions is achieved by multi-stacking PIN junctions in VCSEL; in other words, the high quantum efficiency of solar cells is realized with multi-stacked three p–n-junction structures, considering different wavelength sensitivity in the visible-light wavelength to near-infrared-light wavelength region. Moreover, the multi-junction technique has a potential to reduce junction capacitance in high-speed PD design. Stacking a PIN-PD structure perpendicularly on a surface may reduce junction capacitance.

Fig. 2 shows an energy band diagram of a multi-stacked PIN-PD, which reduces junction capacitance to 50% assuming a double-stacked PIN structure. Between two stacked PIN

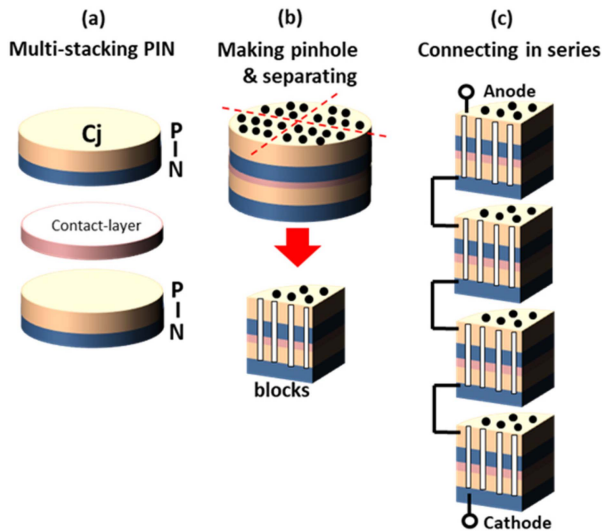


Fig. 3. PD device configuration of the multi-stacked PIN structure, which consists of four blocks connected in series with small pinholes.

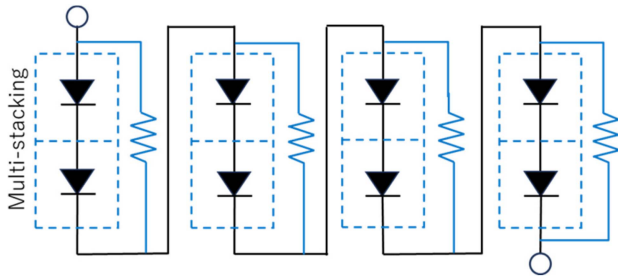


Fig. 4. Equivalent circuit diagram of the fabricated multi-stacked PIN-PD shown in Fig. 3(c).

(p-InP(cap)/i-InGaAs(absorption)/n-InP(cap)) structures, high-doped thin n-InGaAs and p-InGaAs layers were placed to reduce the contact resistance between the two PIN structures. The notch barrier between n-InP in the upper PIN and p-InP in the lower PIN generated resistance in the two-series PIN structure. Applying the reverse bias voltage to the junction, some of the generated carriers would jump over the barrier.

When we assume junction capacitance as  $C_j$  in a conventional large single PIN structure, the overall capacitance in a double-stacked PIN-PD structure should be equal to  $1/2 \times C_j$  (Fig. 3). Fabricating  $5\text{-}\mu\text{m}$  pinholes with a 50% fill factor against a large junction area using dry etching process may result in  $1/4 \times C_j$ . Furthermore, if the two-stacked PIN-PD structures with small pinholes (50% fill factor) are divided into four blocks (Fig. 3(b)), the junction capacitance of each block should be  $1/16$  smaller than  $C_j$  in a conventional large PIN-PD. By connecting the four blocks with an anode and cathode in series, the overall junction capacitance illustrated in Fig. 3(c) should be equal to  $1/64$  smaller than  $C_j$  illustrated in Fig. 3(a). Fig. 4 shows an equivalent circuit model of the designed multi-stacked PIN-PD structure corresponding to Fig. 3(c). A dash square box shown in Fig. 3(c) includes a double-stacked PIN structure with  $5\text{-}\mu\text{m}$  pinholes, and four boxes (blocks) are connected in series. Adding

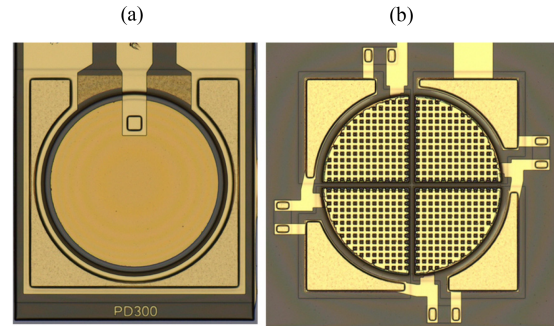


Fig. 5. (a) Photograph of 0.3 mm large aperture conventional PIN-PD (sample-A and A'), (b) photograph of newly developed 0.3 mm multi-stacked PIN-PD (sample-B).

a small shunt resistor to the boxes (blocks) can help bypassing the generated photocurrent through the shunt resistor.

### B. Device Fabrication and Characteristic

We fabricated two kinds of 0.3-mm large-aperture PIN-PDs to consider beam fluctuation while moving the FSO transceiver system. Sample-A: a conventional 0.3-mm large-aperture PD with a single PIN structure (Fig. 5(a)). Sample-B: four blocks with a double-stacked PIN structure and pinholes connected in series (Fig. 5(b)). In the III-V epitaxial growing process, the i-InGaAs absorption layer with a thickness of  $1.2\ \mu\text{m}$  was employed, and a 20-nm thin p-n highly doped InGaAs contact layer was introduced between each PIN structure. After the deposition of ohmic metal as a top contact layer, an n-InP clean surface for the bottom contact layer and  $5\text{-}\mu\text{m}$  pinholes were formed using a chlorine-based etching gas process. The n-InP bottom contact layer was isolated via dry etching. Simultaneously, the thin film resistor shown in Fig. 5(b) was fabricated using the n-InP isolation process, in order to bypass the photocurrent through the resistors when the beam is irradiated to four-PD blocks unevenly. The shunt resistor does not affect the PD responsivity. A sheet resistance of  $100\ \Omega/\square$  was obtained from the thin-film-isolated n-InP material ( $1 \times 10^{18}\ \text{cm}^{-3}$ ), considering a resistance of  $100\ \Omega$  in an area of  $100\ \mu\text{m} \times 100\ \mu\text{m}$ . Assuming the bias voltage of 3–5 V to each stacked PIN layer in consideration of  $1.2\ \mu\text{m}$  thick absorption layer, the leakage current through the four  $100\text{-}\Omega$  resistors was designed to be 15–25 mA. The resistor was not designed for an impedance matching purpose. After coating the polyamide-isolated thin film, the gold wiring process was used to connect the double-stacked PIN blocks. When comparing the 3 dB bandwidth between sample-A and sample-B, 64 times higher 3 dB bandwidth can be ideally expected.

Fig. 6 shows the measurement results of frequency response using a lightwave component analyzer through a bias-tee. The 3 dB bandwidth of 0.2 GHz for sample-A (0.3-mm single PIN-PD in Fig. 5(a)) well agreed with the calculated result. In contrast, it was found that the 3 dB bandwidth (7.6 GHz) of sample-B was 38 times higher than that of sample A. We supposed that the difference between the expected (64 times improvement) and measured (38 times improvement) results might be due

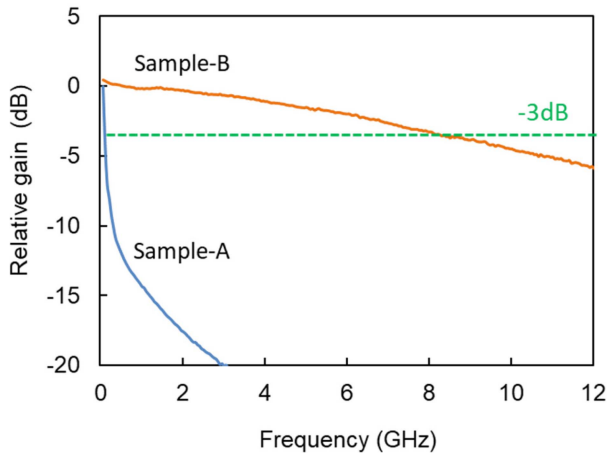


Fig. 6. Measured frequency response: (a) 0.3-mm single PIN-PD (sample-A), (b) 0.3-mm double-stacked PIN-PD consisted of four blocks with pinholes connected in series (sample-B).

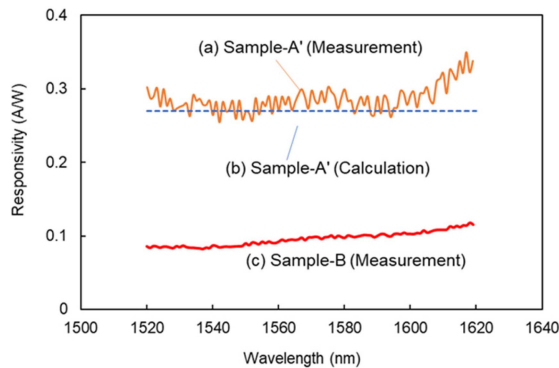


Fig. 7. Spectral responsivity in 1520–1620 nm for (a) double-stacked PIN-PD (measurement, sample-A'), (b) double-stacked PIN-PD (calculation, sample-A'), (c) multi-stacked PIN-PD described in Fig. 5(b) (measurement, sample-B).

to shut resistor affection. Under the low shunt resistor condition ( $100 \Omega$ ), the entire 3 dB bandwidth might be decreased. Moreover, the insufficient pinhole depth in the etching process regarding junction capacitance reduction might be related to the difference as well. The low cut-off frequency was not measured in this experiment.

We evaluated spectral responsivity in the wavelength range of 1520–1620 nm (Fig. 7). The calculated responsivity of sample-A (conventional single PIN structure) was estimated to be as high as  $0.8 \text{ A/W}$  at 1550 nm, assuming InGaAs absorption layer thickness ( $d$ ) to be  $1.2 \mu\text{m}$  and absorption coefficient to be  $1 \times 10^4 \text{ cm}^{-1}$ . Next, the responsivity of sample-A' (double-stacked PIN structure, Fig. 5(a)) was calculated to be as low as  $0.28 \text{ A/W}$ , where the notch barrier affection was not taken into account, because the optical power was absorbed by the first top InGaAs absorption layer and the decayed optical power was absorbed by the second bottom InGaAs layer. The overall photocurrent of sample-A' should be dominated by the lower photocurrent region in the two InGaAs layers. Note: the top and bottom absorption layer thickness was not optimized in this work. The balance between those two layers will be important

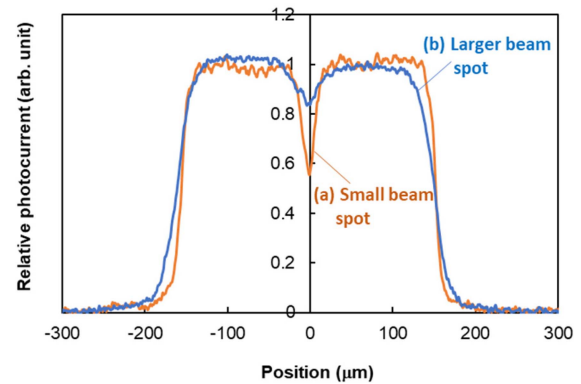


Fig. 8. Photo-current profile when scanning beam spot on the multi-stacked PIN-PD surface, (a) using small beam spot, (b) using larger beam spot.

to increase the responsivity. Fig. 7 shows the good agreement between the calculated and measured results of sample-A'. This also suggested that the notch barrier in the double stacked PIN structure had few affections to the responsivity. According to the measured result of sample-B, the expected photocurrent (responsivity) should be close to the half photocurrent ( $0.14 \text{ A/W}$ ) of sample-A', considering pinholes with a 50% fill factor. Here, the non-photodetection area of the central region may lead to lower responsivity ( $0.1 \text{ A/W}$ ). Although a special pinhole design to increase responsivity was not taken into consideration, it might have a potential to improve the responsivity using lightwave scattering, reflection and photon-trap effect [32] from high-mesa surface at pinhole.

In Fig. 8, we measured the in-plane photocurrent distribution considering different beam spot sizes while scanning the beam positions in the multi-stacked PIN-PD (sample-B; Fig. 5(b)). The photocurrent distribution profile was not affected by  $5\text{-}\mu\text{m}$  pinholes; however, the photocurrent (red line) at the central position considerably decreased owing to the small beam spot, where approximately  $20 \mu\text{m}$  beam size was inferred. The expanded beam size helped mitigate the large drop, as indicated by the blue line.

### III. MOBILE-OWC TRANSCEIVER

#### A. Transceiver Design

Assuming a low-speed short-range mobile OWC scenario, we developed a laser-light based mobile OWC transceiver (called as “FSO transceiver”) equipped with the newly developed multi-stacked PIN-PD. The FSO system was configured via the fiber-to-detector coupling between the transmitter and receiver using 1550-nm laser light. The newly developed mobile optical transceiver is the modified version of the transceiver considered in our previous study [19], [20], which was designed for fiber-to-fiber communication between the transmitter and receiver, and the field of view (FoV) of  $11.5^\circ$  and the moving speed of  $400 \text{ mm/s}$  ( $1.4 \text{ km/h}$ ) were increased herein (Fig. 9(a)). The transceiver comprised three main components: FSO antenna, 2-dimensional (2D) fast steering mirror, and IR camera. To align the coarse laser beam, a beacon LED light ( $940 \text{ nm}$ ) and an IR camera installed with FSO main flame were used. The 2D fast

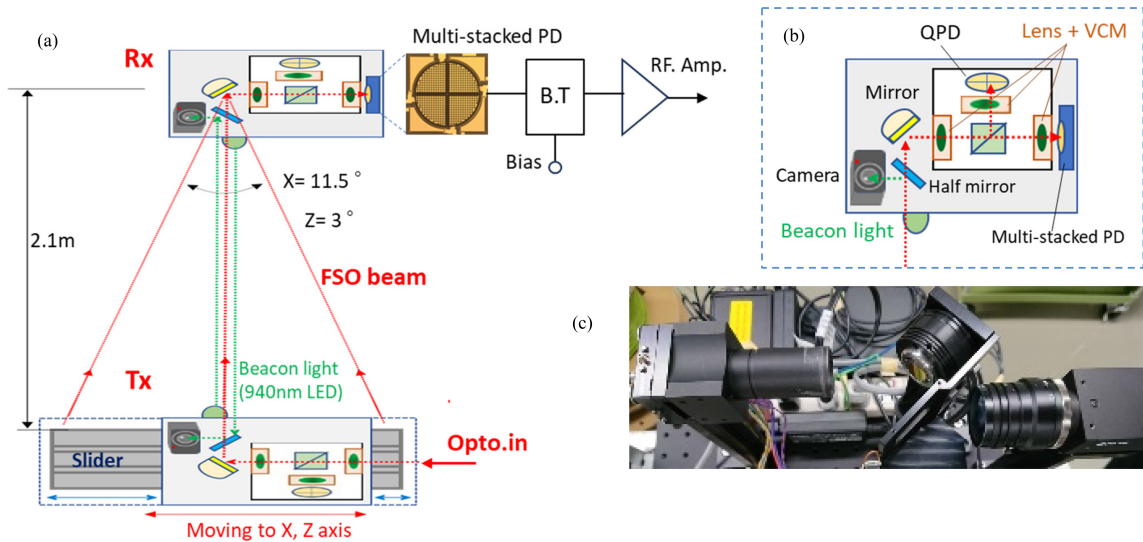


Fig. 9. (a) Experimental setup for mobile FSO communications using the multi-stacked PIN-PD; (b) configuration of the inside of the FSO transceiver; (c) photograph of mobile FSO transceiver.

steering mirror (15 mm diameter) can help change the reflection angle to a moving incident beam angle (Fig. 9(c)). Although the FSO transceiver was moving, the alignment processes ensured that the laser beam was roughly introduced into the FSO antenna. Moreover, a fine beam alignment process and beam tracking process were conducted inside of the FSO antenna. In the small FSO antenna body (10 cm (W)  $\times$  5 cm (H)  $\times$  5 cm (D)), four movable lenses attached to 3-axis voice-coil motors (VCMs) were installed for fast auto-focusing as a key component. The fast-tracking latency of  $<5$  ms was realized using the newly developed beam control and prediction software tool. In the inside of the FSO antenna (Fig. 9(b)), a top VCM for correcting incident beam angle and a medium VCM for beam positioning using a quadrature PD, and final two VCMs for beam alignment in the x and y axes to the multi-stacked PD were configured, respectively. On the transmitter side, FSO transceivers were placed on a mechanical slider, which was controlled by a PC to define the moving speed and position, where the moving stroke in the x and z axes were 0.4 and 0.1 m, respectively. On the receiver side, the location of the FSO transceiver with the 0.3-mm large multi-stacked PD was fixed. The distance between the transmitter and receiver was set to 2.1 m to confirm the proposed mobile FSO design concept. The mechanical slider could move at 0–400 mm/s (0–1.4 km/h), which corresponded to the relative moving speed of 13.7 km/h at 20 m. The FoVs of this system were as wide as  $11.5^\circ$  along the x axis (horizontal direction) and  $3^\circ$  along the z axis (vertical direction).

### B. Performance

First, we evaluated the beam-tracking capability of our fabricated mobile FSO system. While the beam was shifted toward the x axis at 400 mm/s on the transmitter side, the photocurrent was recorded considering different aperture sizes of the PDs on the receiver side for 50 s, where commercially available PDs

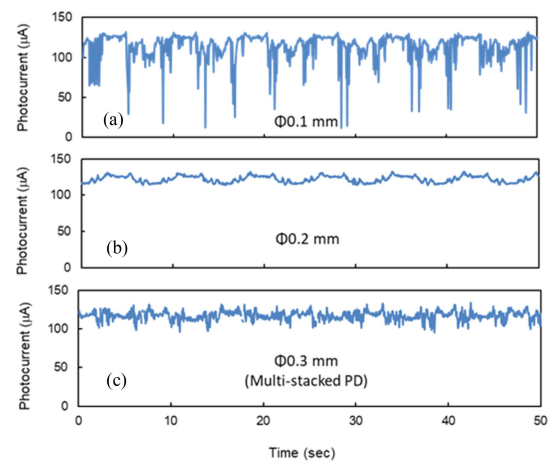


Fig. 10. Measured photocurrent while moving transceivers with different PD sizes: (a) 0.1 mm diameter; (b) 0.2 mm diameter; (c) 0.3-mm multi-stacked PIN-PD.

with diameters of 0.1 and 0.2 mm and the newly developed multi-stacked PIN-PD with a diameter of 0.3 mm were used herein. The DC photocurrent generated by the 1550-nm CW laser light was recorded at a sampling rate of 20 sps. The minimum beam spot size obtained on the PD surface was approximately  $20 \mu\text{m}$ ; however, it mainly depended on the focal point, as discussed in the previous section. Here, as long as the beam position fluctuated within the photodetection area on the PD surface, the photocurrent level remained constant during the recording period.

As shown in Fig. 10(a), photocurrent level in 50 s recording time was considerably fluctuated and decreased for the PD with a diameter of 0.1 mm. It suggested that the moving beam was not tracked properly, and the beam position was located in the outlier of the 0.1 mm PD aperture. Employing a PD aperture less than 0.1 mm diameter was not suitable for our mobile FSO system. Increasing the PD aperture size to 0.2 mm diameter, the recorded photocurrent in 50 s. was stable with small

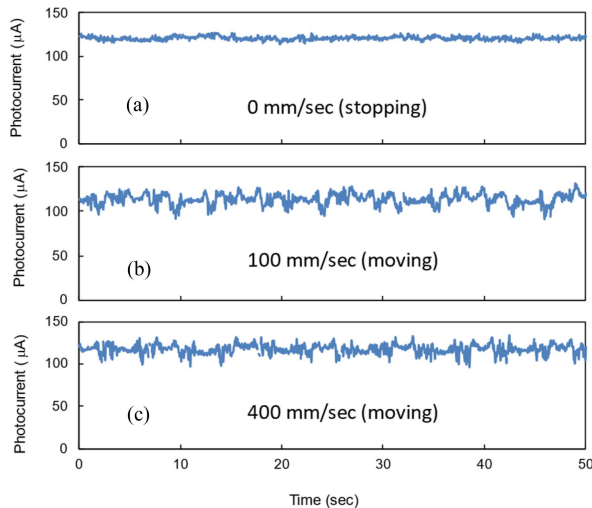


Fig. 11. Measured photocurrent of the 0.3-mm multi-stacked PIN-PD while moving transceivers at (a) 0 km/h (stopping), (b) 100 mm/s (0.4 km/h), and (c) 400 mm/s (1.4 km/h).

periodic fluctuation (Fig. 10(b)). Therefore, the diameter of the PD aperture in our mobile FSO system should be more than 0.2 mm. Replacing the 0.3 mm multi-stacked PD, photocurrent stability was analyzed as well. Although no considerable drops were observed (Fig. 10(c)), very small spikes (approximately 10% variation) were observed, as the unsensitive region was located in the center of the multi-stacked PD. However, we thought that the affection of 10% fluctuation to communications would be very few. Moreover, the recorded DC photocurrents at 0, 100, and 400 mm/s in the multi-stacked PD were compared (Fig. 11(a)–(c)). While stopping the beam movement (0 mm/s; Fig. 11(a)), no spike in the photocurrent was observed. While moving the beam, we revealed that the photocurrent variation level at 400 mm/s (Fig. 11(c)) was almost the same as that at 100 mm/s (Fig. 11(b)), indicating that the beam-tracking function of the mobile FSO system can be operated well at up to 400 mm/s.

#### IV. MOBILE-OWC DEMONSTRATION

To confirm the proof of concept for the mobile-FSO transceiver with the multi-stacked large PD, optical wireless communication in free space of 2.1 m was demonstrated at 10–20 Gbps (OOK), considering a 3 dB bandwidth of 7.6 GHz. In the experimental setup, as shown in Fig. 9, the optical input to the FSO receiver was directly coupled to the PD, which was biased from a bias-tee, and the RF output signal was amplified using an RF amplifier. While stopping the transceiver, a clear eye with a large opening was obtained at 10 Gbps (left inset in Fig. 12), and it degraded at 20 Gbps (right inset in Fig. 12) owing to the short 3 dB bandwidth.

According to the measured BER results (Fig. 12), a straightforward BER curve at 10 Gbps was observed, and an optical power of  $-3$  dBm was required at  $\text{BER} = 1 \times 10^{-6}$ . At 20 Gbps, a power penalty of 7 dB was observed against 10 Gbps at  $\text{BER} = 1 \times 10^{-6}$ . However, the characteristic derived at 20 Gbps had the potential to obtain a BER of  $< 1 \times 10^{-6}$ .

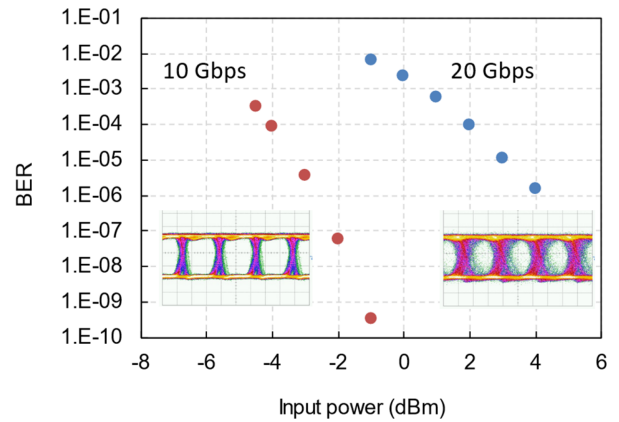


Fig. 12. Measured BER results at 10 and 20 Gbps, while stopping the transceiver, with eye diagrams (inset).

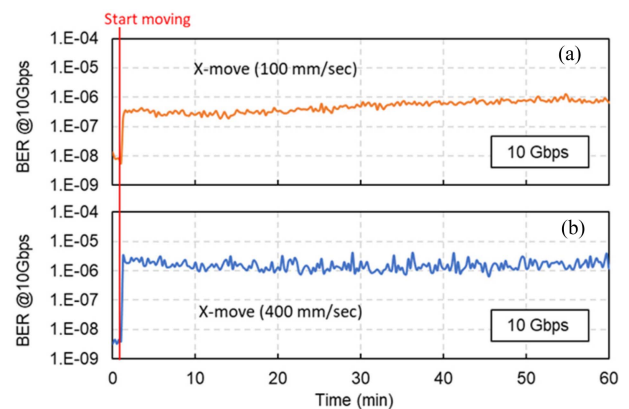


Fig. 13. Measured BER results at 10 Gbps, while moving the transceiver (a) at 0.4 and (b) 1.4 km/h.

While moving the transceiver at 100 mm/s (0.4 km/h) and 400 mm/s (1.4 km/h), the BER measurement results at 10 Gbps and  $-1.5$  dBm were recorded in 60 min, where the sampling time for recording was 30 s. The BER level of  $10^{-8}$ – $10^{-9}$  before moving the transceiver was changed to  $10^{-6}$ – $10^{-7}$  level after moving the transceiver. However, these measured BER results were sufficiently lower than  $3.8 \times 10^{-3}$  (7% forward error correction level). Comparing two moving conditions, the BER was more stable at 100 mm/s (Fig. 13(a) and (b)).

Next, at 20 Gbps and  $+3$  dBm, the BER was measured and recorded in 60 min, where the moving speed was set to 400 mm/s. The BER level was degraded to the  $10^{-3}$  range; however, it was still maintained at  $< 3.8 \times 10^{-3}$  (Fig. 14(a)). Moreover, when modifying the moving direction from the x axis to the x–z axis (zigzag movements), the BER was measured and recorded (Fig. 14(b)). We found very few differences between those two conditions (the zigzag moving and the x-axis moving conditions). Therefore, the newly developed mobile-FSO system attached to the multi-stacked PD can achieve 1D and 2D beam tracking and detection.

#### V. CONCLUSION

We designed and fabricated a multi-stacked 0.3-mm large-aperture PIN-PD operated up to 20 Gbps to mitigate optical

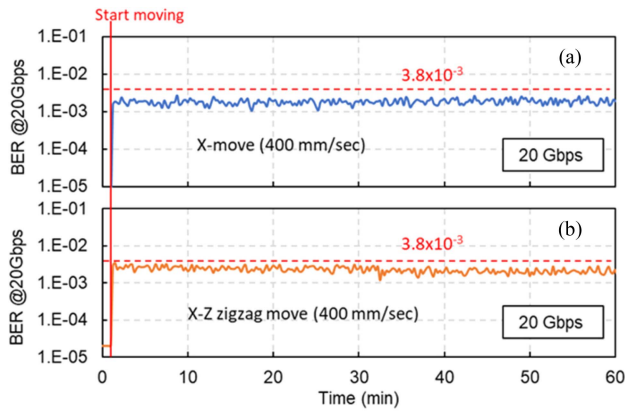


Fig. 14. Measured BER results at 20 Gbps, while moving the transceiver at 1.4 km/h (a) toward the horizontal direction and (b) horizontal-vertical direction (zigzag).

alignment tolerance in a mobile OWC system, which comprised two n-InP/InGaAs/p-InP structures connected by a contact layer. During fabrication, the multi-stacked epitaxial layer was divided into four blocks containing small pinholes with a 50% fill factor, and each block was connected in series to reduce PIN junction capacitance. We successfully confirmed a 38 times higher 3 dB bandwidth (7.6 GHz) compared to a conventional 0.3-mm large PD via the experiments. To optimize the pinhole etching process or the photo-current bypass circuit design, the 3 dB bandwidth will be increased to  $>10$  GHz. With respect to future improvement of the 3 dB bandwidth (responsivity), stacking additional PIN layers will be one of good approaches. Here, a device structure that applies even internal electric field to each PIN layer will be required. Moreover, in addition to the stacking layer technique, dividing and cascading the divided sections in series will be one of promising approaches to increase 3 dB bandwidth. Here, because the number of dividing sections allows increasing non-photo-detective area, precise and fine semiconductor processes will be required to achieve it.

While scanning the beam spot across the photodetection area, it was found that the large drop in the photocurrent profile located in the central region was mitigated owing to the change in the beam spot size from a focused small beam spot to an expanded one. Assuming 10–20 km/h mobile communication applications in short distance, a mobile FSO transceiver combined with a newly developed multi-stacked PIN-PD, which exhibits a fast-tracking function using a fast movable lens, was designed and fabricated to operate well at a moving speed of 400 mm/s (1.4 km/h) at 2.1 m, which corresponded to 13.7 km/h relative speed at 20 m. The beam-tracking function in the mobile FSO transceiver, with an FoV of  $11.5^\circ$  along the x axis and  $3^\circ$  along the z axis, can operate with a large PD possessing an aperture size of 0.2 mm. We successfully achieved BER levels of  $10^{-6}$  at 10 Gbps and  $<3.8 \times 10^{-3}$  at 20 Gbps at a moving speed of 400 mm/s for 1 hour. The received power of  $-1.5$  dBm and  $+3$  dBm at 10 Gbps and 20 Gbps will be improved by optimizing the multi-stacked PIN-PD structure.

## ACKNOWLEDGMENT

The authors would thank all the technical staff members of the photonic device laboratory in NICT for supporting the fabrication process.

## REFERENCES

- [1] Society 5.0, Japanese Cabinet Office site, 2021. [Online]. Available: [https://www8.cao.go.jp/cstp/english/society5\\_0/index.html](https://www8.cao.go.jp/cstp/english/society5_0/index.html)
- [2] 4G Wireless Broadband Industry WHITE PAPER, 2017. [Online]. Available: [https://www-file.huawei.com/-/media/corporate/pdf/news/4g-wireless-broadband-industry-white-paper.pdf?la=en&source=corp\\_comm](https://www-file.huawei.com/-/media/corporate/pdf/news/4g-wireless-broadband-industry-white-paper.pdf?la=en&source=corp_comm)
- [3] DOCOMO 5G White Paper, “5G radio access: Requirements, concept and technologies,” Jul. 2014. [Online]. Available: [https://www.docomo.ne.jp/english/binary/pdf/corporate/technology/whitepaper\\_5g/DOCOMO\\_5G\\_White\\_Paper.pdf](https://www.docomo.ne.jp/english/binary/pdf/corporate/technology/whitepaper_5g/DOCOMO_5G_White_Paper.pdf)
- [4] DOCOMO White Paper, “5G evolution and 6G,” Version 5.0, Jan. 2023. [Online]. Available: [https://www.docomo.ne.jp/english/binary/pdf/corporate/technology/whitepaper\\_6g/DOCOMO\\_6G\\_White\\_PaperEN\\_v5.0.pdf](https://www.docomo.ne.jp/english/binary/pdf/corporate/technology/whitepaper_6g/DOCOMO_6G_White_PaperEN_v5.0.pdf)
- [5] M. G. L. Frecassetti et al., “D-band radio solutions for beyond 5G reconfigurable meshed cellular networks,” in *Proc. 16th Int. Symp. Wireless Commun. Syst.*, 2019, pp. 427–431.
- [6] F. Taleb, G. G. Hernandez-Cardoso, E. Castro-Camus, and M. Koch, “Transmission, reflection, and scattering characterization of building materials for indoor THz communications,” *IEEE Trans. Terahertz Sci. Technol.*, vol. 13, no. 5, pp. 421–430, Sep. 2023.
- [7] N. Khalid and O. B. Akan, “Experimental throughput analysis of low-THz MIMO communication channel in 5G wireless networks,” *IEEE Wireless Commun. Lett.*, vol. 5, no. 6, pp. 616–619, Dec. 2016.
- [8] Y. Hong et al., “Demonstration of  $>1$  Tbit/s WDM OWC with wavelength-transparent beam tracking-and-steering capability,” *Opt. Exp.*, vol. 29, no. 21, pp. 33694–33702, Oct. 2021.
- [9] X. Sun, L. Yu, and T. Zhang, “Latency aware transmission scheduling for steerable free space optics,” *IEEE Trans. Mobile Comput.*, vol. 22, no. 4, pp. 2221–2232, Apr. 2023.
- [10] L. Wu and P. Wang, “Channel interference technology research based on wireless communication network,” in *Proc. IEEE Int. Conf. Power Electron., Comput. Appl.*, 2021, pp. 1028–1031, doi: [10.1109/ICPECA51329.2021.9362639](https://doi.org/10.1109/ICPECA51329.2021.9362639).
- [11] M. Hussain, Q. Du, L. Sun, and P. Ren, “Security protection over wireless fading channels by exploiting frequency selectivity,” in *Proc. 8th Int. Conf. Wireless Commun. Signal Process.*, 2016, pp. 1–5, doi: [10.1109/WCSP.2016.7752566](https://doi.org/10.1109/WCSP.2016.7752566).
- [12] H. Kaushal and G. Kaddoum, “Optical communication in space: Challenges and mitigation techniques,” *IEEE Commun. Surv. Tuts.*, vol. 19, no. 1, pp. 57–96, Firstquarter 2017.
- [13] J. He, L. Wang, X. Chang, and Q. Xie, “Fiber coupling efficiency of partially coherent Gaussian beam in ground-to-HAP free-space optical communication systems,” in *Proc. 8th Int. Conf. Comput. Commun. Syst.*, 2023, pp. 510–514.
- [14] A. Fayad, T. Cinkler, and J. Rak, “5G/6G optical fronthaul modeling: Cost and energy consumption assessment,” *J. Opt. Commun. Netw.*, vol. 15, no. 9, pp. D33–D46, Sep. 2023.
- [15] Z. Zhang et al., “Optical mobile communications: Principles and challenges,” in *Proc. 26th Wireless Opt. Commun. Conf.*, 2017, pp. 1–4, doi: [10.1109/WOCC.2017.7928992](https://doi.org/10.1109/WOCC.2017.7928992).
- [16] T. Koonen, “Indoor optical wireless systems: Technology, trends, and applications,” *J. Lightw. Technol.*, vol. 36, no. 8, pp. 1459–1467, Apr. 2018.
- [17] Press release, softbank news, “SoftBank and nikon utilize light to broaden the potential of telecommunications,” Apr. 2021. [Online]. Available: [https://www.softbank.jp/en/sbnews/entry/20210420\\_01](https://www.softbank.jp/en/sbnews/entry/20210420_01)
- [18] Z. Zeng, S. Fu, H. Zhang, Y. Dong, and J. Cheng, “A survey of underwater optical wireless communications,” *IEEE Commun. Surv. Tuts.*, vol. 19, no. 1, pp. 204–238, Firstquarter 2017.
- [19] A. Bekkali, H. Fujita, and M. Hattori, “New generation free-space optical communication systems with advanced optical beam stabilizer,” *J. Lightw. Technol.*, vol. 40, no. 5, pp. 1509–1518, Mar. 2022.
- [20] A. Bekkali, H. Fujita, M. Hattori, Y. Hara, T. Umezawa, and A. Kanno, “All-optical mobile FSO transceiver with high-speed laser beam steering and tracking,” in *Proc. Eur. Conf. Opt. Commun.*, 2022, pp. 1–4.

- [21] T. Umezawa, T. Sakamoto, A. Kanno, N. Yamamoto, and T. Kawanishi, "High speed 2-D photodetector array for space and mode-division multiplexing fiber communications," *J. Lightw. Technol.*, vol. 36, no. 17, pp. 3684–3692, Sep. 2018.
- [22] T. Umezawa et al., "FSO receiver with high optical alignment robustness using high-speed 2D-PDA and space diversity technique," *J. Lightw. Technol.*, vol. 39, no. 4, pp. 1040–1047, Feb. 2021.
- [23] T. Umezawa et al., "Resonant cavity 4- $\lambda$  integrated 4  $\times$  4 PD-array for high optical alignment robustness WDM-FSO communications," *J. Lightw. Technol.*, vol. 41, no. 8, pp. 2465–2473, Apr. 2023.
- [24] T. Umezawa, A. Matsumoto, K. Akahane, S. Nakajima, and N. Yamamoto, "Large submillimeter high-speed photodetector for large aperture FSO receiver," *IEEE J. Sel. Topics Quantum Electron.*, vol. 28, no. 2, Mar./Apr. 2022, Art. no. 3801709.
- [25] T. Umezawa, A. Matsumoto, K. Akahane, A. Kanno, and N. Yamamoto, "400-pixel high-speed photodetector for high optical alignment robustness FSO receiver," in *Proc. Opt. Fiber Commun. Conf. Exhib.*, 2022, pp. 01–03.
- [26] T. Umezawa et al., "Multi-stacked large-aperture high-speed PIN-photodetector for mobile-FSO communication," in *Proc. Eur. Conf. Opt. Commun.*, 2023, Paper We.D.1.2.
- [27] F.-M. Kuo, M.-Z. Chou, and J.-W. Shi, "Linear-cascade near-ballistic untraveling-carrier photodiodes with an extremely high saturation-current-bandwidth product," *J. Lightw. Technol.*, vol. 29, no. 4, pp. 432–438, Feb. 2011.
- [28] A. Ghods, M. Dummer, G. Xu, and K. Johnson, "Design and fabrication of single-mode multi-junction 905 nm VCSEL with integrated anti-phase mode filter," *J. Lightw. Technol.*, vol. 41, no. 10, pp. 3102–3107, May 2023.
- [29] S. Xie et al., "High-power and high-speed multi-junction VCSEL arrays for automotive LiDAR," in *Proc. IEEE Photon. Conf.*, 2022, pp. 1–2, doi: [10.1109/IPC53466.2022.9975568](https://doi.org/10.1109/IPC53466.2022.9975568).
- [30] W. Guter and A. W. Bett, "I-V characterization of tunnel diodes and multijunction solar cells," *IEEE Trans. Electron Devices*, vol. 53, no. 9, pp. 2216–2222, Sep. 2006.
- [31] R. Núñez et al., "Spectral impact on multijunction solar cells obtained by means of component cells of a different technology," *IEEE J. Photovolt.*, vol. 8, no. 2, pp. 646–653, Mar. 2018.
- [32] C. Bartolo-Perez et al., "Avalanche photodetectors with photon trapping structures for biomedical imaging applications," *Opt. Exp.*, vol. 29, no. 12/7, pp. 19024–19033, 2021.

**Toshimasa Umezawa** (Member, IEEE) received the B.E. and M.E. degrees in electronics from Nagaoka University, Niigata, Japan, in 1984 and 1986, respectively, and the Ph.D. degree in electronics from Tokyo University, Tokyo, Japan, in 1995. From 1987 to 2011, he was with the Yokogawa Electric Corporation; he was with the Central Research Laboratory and with the Photonics Business Department. In 1992, he was a Visiting Scholar with the Department of Applied Physics, Stanford University, Stanford, CA, USA. He was engaged in research on superconductor devices, photonics devices, and their applications with Tokyo University. In 2011, he joined the National Institute of Information and Communications Technology, Tokyo, Japan. He is a member of the Institute of Electronics, Information, and Communication Engineers, and the Japan Society of Applied Physics. His research interests include E/O devices and photonic integrated circuits and millimeter-wave photonics.

**Shinya Nakajima** received the B.E. degree in electrical engineering from Nihon University, Tokyo, Japan, in 2001. He was with Asami Electric Company, Ltd., and Link Tomorrow Company, Ltd. with the Optical Device Technology Center. In 2006, he joined the National Institute of Information and Communications Technology, NICT, Tokyo, where he is currently with a Technical Engineer. He has been engaged in the design, fabrication, packaging, and evaluation of high-frequency optical devices.

**Abdelmoula Bekkali** (Senior Member, IEEE) received the M.Sc. and Ph.D. degrees from Waseda University, Tokyo, Japan, in 2007 and 2010, respectively. He was a Senior Researcher with KDDI Research Inc. during 2014–2019, an Adjunct Lecturer with Waseda University during 2012–2019, a Research Scientist with Qatar Mobility Innovation Center (QMIC), Qatar, during 2011–2014, and a Researcher with NTT Labs, Tokyo, during 2010–2011. He is currently a R&D Manager with TOYO Electric Corporation, Japan, where he is leading the development of next generation FSO systems for fixed and mobile platforms. He holds ten granted Japanese patents in the field of optical and wireless communications. His research interests include optical wireless communication, free-space optics systems, fiber-wireless systems, millimeter-wave communications, and RFID systems. He was the recipient of the 2016 KDDI Excellent Research Award, 2009 Waseda University Ono Azusa memorial Gold medal, 26th Telecom System Technology Award from the Telecommunication Advancement Foundation (TAF) of Japan, and Best Paper Awards of IEICE Transactions in 2009 and 2015, IIEEJ Journal in 2012, and IEEE WCNC Conference in 2014. He was the ONS Symposium Co-Chair of IEEE Globecom 2020.

**Michikazu Hattori** received the graduation degree from the Faculty of Engineering, Aichi Institute of Technology, Toyota, Japan, in 1989. In 1994, he joined TOYO Electric Corporation, where he is currently a R&D Manager. He is also leading several R&D projects and commercial products related to free-space optics and underwater visible light communications. He is a Member of Institute of Electronics, Information, and Communication Engineers.

**Atsushi Matsumoto** (Member, IEEE) received the B.S. degree in electronics, information, and communication engineering, and the M.S. and Dr. Eng. degrees in electrical engineering and bioscience from Waseda University, Tokyo, Japan, in 2003, 2005, and 2015, respectively. He is currently the Senior Researcher of National Institute of Information and Communications Technology (NICT), Tokyo. He is a member of the Japan Society of Applied Physics and the Institute of Electronics, Information and Communication Engineers of Japan.

**Atsushi Kanno** (Senior Member, IEEE) received the B.Sci., M.Sci., and Ph.D. degree in science from the University of Tsukuba, Japan, in 1999, 2001, and 2005, respectively. In 2005, he was with the Venture Business Laboratory of the Institute of Science and Engineering, University of Tsukuba. In 2006, he joined the National Institute of Information and Communications Technology (NICT), Japan. Since 2022, he has been with the Nagoya Institute of Technology, Japan. His research interests include microwave photonics and broadband optical and radio communication systems and their sensing applications. He is a member of the Institute of Electronics, Information and Communication Engineers, Japan Society of Applied Physics, Laser Society of Japan, and SPIE.

**Kouichi Akahane** received the B.E., M.E., and Ph.D. degrees in materials science from the University of Tsukuba, Japan, in 1997, 1999, and 2002, respectively. In 2002, he joined the Communications Research Laboratory, Tokyo, Japan. Since 2004, he has been with the National Institute of Information and Communications Technology, Tokyo. He is currently the Director of Optical Access Technology Laboratory, National Institute of Information and Communications Technology. He is also working on semiconductor photonic devices.

**Naokatsu Yamamoto** received the Ph.D. degree in electrical engineering from Tokyo Denki University, Tokyo, Japan, in 2000. In 2001, he joined the National Institute of Information and Communications Technology (NICT). He also joined Tokyo Denki University as a Visiting Professor in 2008 and the Ministry of Internal Affairs and Communications (MIC) as the Deputy Director from 2012 to 2013. Since 2016, he has managed a network science and convergence device technology laboratory in NICT and also has been the Director of advanced ICT Device Laboratory. His research interests include a heterogeneous quantum dot laser with silicon photonics, a convergence device technology of photonics and wireless, and the use of a 1.0- $\mu\text{m}$  waveband (thousand-band, T-band) as a new optical frequency band for short-range communications.